Advances in Difference Equations
a SpringerOpen Journal

Approximation of linear one dimensional partial differential equations including fractional derivative with non-singular kernel

Raheel Kamal[1], Kamran[1], Gul Rahmat[1], Ali Ahmadian[2], Noreen Izza Arshad[3] and Soheil Salahshour[4,5*]

*Correspondence:
soheilsalahshour@yahoo.com
[4]Young Researchers and Elite Club,
Mobarakeh Branch, Islamic Azad
University, Mobarakeh, Iran
[5]Faculty of Engineering and Natural
Sciences, Bahcesehir University,
Istanbul, Turkey
Full list of author information is
available at the end of the article

Abstract

In this article we propose a hybrid method based on a local meshless method and the Laplace transform for approximating the solution of linear one dimensional partial differential equations in the sense of the Caputo–Fabrizio fractional derivative. In our numerical scheme the Laplace transform is used to avoid the time stepping procedure, and the local meshless method is used to produce sparse differentiation matrices and avoid the ill conditioning issues resulting in global meshless methods. Our numerical method comprises three steps. In the first step we transform the given equation to an equivalent time independent equation. Secondly the reduced equation is solved via a local meshless method. Finally, the solution of the original equation is obtained via the inverse Laplace transform by representing it as a contour integral in the complex left half plane. The contour integral is then approximated using the trapezoidal rule. The stability and convergence of the method are discussed. The efficiency, efficacy, and accuracy of the proposed method are assessed using four different problems. Numerical approximations of these problems are obtained and validated against exact solutions. The obtained results show that the proposed method can solve such types of problems efficiently.

Keywords: Local meshless method; Linear partial differential equations; Laplace transform; Caputo Fabrizio fractional derivative

1 Introduction

The integer order derivatives are local in nature, i.e., using these derivatives changes in a neighborhood of a point can be described, but using the arbitrary order derivatives we can describe changes in an interval. Namely, fractional derivatives are nonlocal in nature. That is why arbitrary order derivatives are suitable to model more physical phenomena such as electrodynamics, earthquake vibrations, diffusion process, polymers, fluid flow, elasticity, hydrology, and signal and image processing [1–7]. Fractional order derivative of a function is in fact its definite integral. A geometrically fractional derivative accumulates the function. The corresponding accumulation includes the integer order derivative as a special case. In the literature a large number of arbitrary order derivatives are available such as the Marchaud, Grünwald–Letnikov, Riemann–Liouville, and Caputo derivatives

[8–15]. However, these derivatives have certain disadvantages, these derivatives contain kernels with singularities. It is reported in the literature that these derivatives face problems when someone tries to model nonlocal phenomenon [1, 16]. Therefore, to model the non-local phenomenon accurately, recently a new fractional derivative has been defined, called the Caputo–Fabrizio (CF) derivative [17].

The research community took great interest in the CF derivative due to its non-singular kernel. The CF derivative has a large number of applications, and researchers have applied it successfully to many phenomena like signal processing [18], ground water pollution [19], groundwater flow in a confined aquifer [1, 20], the mass–spring damper system [21], non-Darcian flow and solute transport [22].

In many real world problems as regards their modeling, we need to obtain their exact solution which is some times quite difficult specially for nonlinear problems. Therefore, we need some sophisticated tools to deal with such problems. The researchers increasingly have used numerical and analytical techniques to handle the problems for corresponding numerical and analytical solutions. For example a homotopy analysis method based on the Laplace transform is proposed for solving linear problems including the CF derivative in [2, 23]. In [1] the authors solved the model of groundwater flow with the CF derivative using the Sumudu transform. In [24] a fractional order Fisher diffusion equation with the CF derivative is solved via some iterative method. The Crank–Nicholson scheme in [25] is applied for approximating the solution of the Allen Cahn model with CF derivative. A numerical approximation of the solution of groundwater pollution model with space–time fractional CF derivative in [19] is obtained via the Crank–Nicholson scheme. The Laplace and Fourier transforms are utilized in [26] for obtaining the fundamental solution of advection–diffusion equation with the CF derivative. In [27] the authors applied the CF derivative to the analysis of a rock fracture process. Many other numerical and analytical techniques for the solutions of different fractional order models can be found in [28–39] and the references therein. In this work our aim is to approximate linear PDEs with the CF derivative via the Laplace transform (LT) and local meshless method. The Laplace transform is coupled with a local meshless method for avoiding the time stepping procedure. The Laplace transform will help us in obtaining the solution in less computation time and without time instability. The paper is organized as follows: In Sect. 2 some basic definitions are given; In Sect. 3 the Laplace transform and contour integration methods are discussed; Sect. 3.1 shows how to construct the differentiation matrices via a local meshless method; Sect. 4 discusses the convergence of the method; Sect. 5 discusses the stability of the method; Sect. 6 contains the numerical tests, where theory and experiment are compared.

2 Preliminaries

Definition 2.1 The LT of a piecewise continuous function $f(t)$, $t > 0$ is defined as

$$\mathscr{L}\big[f(t)\big] = \hat{f}(s) = \int_0^\infty e^{-st} f(t)\, dt. \tag{1}$$

Definition 2.2 The CF derivative of fractional order α is defined as [17]

$$_{0}^{CF}D_t^\alpha f(t) = \frac{(2-\alpha)B(\alpha)}{2(1-\alpha)} \int_0^t \exp\left(\frac{-\alpha(t-s)}{1-\alpha}\right) \frac{d^n f(s)}{ds^n}\, ds, \quad \alpha \in (n-1, n), \tag{2}$$

where $B(\alpha)$ denotes the normalization function, satisfying $B(0) = B(1) = 1$.

Definition 2.3 If $n \in \mathbb{N}$, and $0 \leq \alpha \leq 1$ then the LT of the CF fractional derivative is defined as [2, 24]

$$\mathscr{L}\left[{}_0^{CF}D_t^{\alpha+n}f(t)\right](s) = \frac{s^{n+1}\hat{f}(s) - s^n f(0) - s^{n-1}f'(0) - \cdots - f^n(0)}{s + \alpha(1-s)}, \tag{3}$$

using $n = 0$ we get

$$\mathscr{L}\left[{}_0^{CF}D_t^{\alpha}f(t)\right](s) = \frac{s\hat{f}(s) - f(0)}{s + \alpha(1-s)}, \tag{4}$$

and for $n = 1$ we have

$$\mathscr{L}\left[{}_0^{CF}D_t^{\alpha+1}f(t)\right](s) = \frac{s^2\hat{f}(s) - sf(0) - f'(0)}{s + \alpha(1-s)}. \tag{5}$$

3 Numerical scheme

In order to validate our method let us consider a linear one dimensional partial differential equation with the CF derivative for $q - 1 < \alpha + n \leq q$:

$$_0^{CF}D_t^{\alpha}u(x,t) + \mathcal{L}u(x,t) = h(x,t), \quad x \in \Omega, \text{and } 0 \leq t \leq T, \tag{6}$$

the boundary and initial conditions are

$$\partial_t^l u(x,0) = u_l(x), \quad l = 0,1,2,\ldots,q-1,$$

and

$$\mathcal{B}u(x,t) = g(x,t), \quad x \in \partial\Omega, \tag{7}$$

where $\mathcal{L}$ is the linear differential operator and $\mathcal{B}$ is the boundary operator. Applying the LT to Eq. (6) and Eq. (7), we have

$$\mathscr{L}\left[{}_0^{CF}D_t^{\alpha+n}u(x,t) + \mathcal{L}u(x,t)\right] = \mathscr{L}\left[h(x,t)\right] \tag{8}$$

and

$$\mathcal{B}\hat{u}(x,s) = \hat{g}(x,s). \tag{9}$$

From Eq. (8), we have

$$\frac{s^{n+1}\hat{u}(x,s) - s^n u(x,0) - s^{n-1}u'(x,0) - \cdots - u^n(x,0)}{s + \alpha(1-s)} + \mathcal{L}\hat{u}(x,s) = \hat{g}(x,s), \tag{10}$$

on simplification we get

$$\left[\left(\frac{s^{n+1}}{s(1-\alpha) + \alpha}\right)I + \mathcal{L}\right]\hat{u}(x,s) = \hat{\mathcal{G}}(x,s), \tag{11}$$

$$\mathcal{B}\hat{u}(x,s) = \hat{g}(x,s),\tag{12}$$

where $\hat{\mathcal{G}}(x,s)$ is

$$\hat{\mathcal{G}}(x,s) = \frac{s^n u(x,0) + s^{n-1} u'(x,0) + \cdots + u^n(x,0)}{s(1-\alpha) + \alpha} + \hat{g}(x,s).$$

We obtain the solution $u(x,t)$ of (6)–(7) by representing it as an integral along a smooth curve as

$$u(x,t) = \frac{1}{2\pi i} \int_{\sigma - \iota\infty}^{\sigma + \iota\infty} e^{st} \hat{u}(x,s)\,ds = \frac{1}{2\pi i} \int_{\Gamma} e^{st} \hat{u}(x,s)\,ds, \quad \sigma > \sigma_0,\tag{13}$$

where $\sigma_0 \in \mathbb{R}$ is the convergence abscissa, it is large enough and the contour Γ is a suitably selected line Γ_0 perpendicular to x axis connecting $\sigma - \iota\infty$ and $\sigma + \iota\infty$. Then in Eq. (13), $u(x,t)$ is the inverse Laplace of $\hat{u}(x,s)$, with the condition that the Γ_0 lie to the right of all the singularities of the transform $\hat{u}(x,s)$. For our purposes, however, we assume that $\hat{u}(x,s)$ may be continued analytically in an appropriate way. We shall want to take for Γ_0 a deformed contour Γ in the set $\Sigma_\phi^\delta = \{0\} \cup \{s \neq 0 : |\arg s| < \phi\}$. The deformed contour will show asymptotic behavior like the couple of lines in the left half complex plane with $\mathrm{Im}\,s \to \pm\infty$ and $\mathrm{Re}\,s \to -\infty$, forcing the factor e^{st} to decay in the direction of both ends of the contour Γ. In this work we select Γ with the parametric representation of the form [40]

$$s(\boldsymbol{\mu}) = \delta + \xi - \xi \sin(\theta - \iota\boldsymbol{\mu})), \quad \boldsymbol{\mu} \in \mathbb{R},\tag{14}$$

where

$$0 < \theta < \phi - \frac{\pi}{2}, \quad \xi > 0, \quad \text{and} \quad \delta > 0.\tag{15}$$

Letting $s = x + \iota y$, we notice that Eq. (14) serves as the left part of the hyperbola defined by

$$\left(\frac{x - \delta - \xi}{\xi \sin\theta}\right)^2 - \left(\frac{y}{\xi \cos\theta}\right)^2 = 1,\tag{16}$$

where for Eq. (16) the asymptotes are $y = \pm(x - \delta - \xi)\cot\theta$, and its x-intercept is $s = \delta + \xi(1 - \sin\theta)$. Equation (15) ensures that the contour Γ lies in $\Sigma_\phi^\delta = \delta + \Sigma_\phi \subset \Sigma_\phi$, and extends towards the left half complex plane. Using Eq. (14) in Eq. (13) we have

$$u(x,t) = \frac{1}{2\pi \iota} \int_{-\infty}^{\infty} e^{s(\boldsymbol{\mu})t} \hat{u}\big(x,s(\boldsymbol{\mu})\big) s'(\boldsymbol{\mu})\,d\boldsymbol{\mu}.\tag{17}$$

The approximation of Eq. (17) can be obtained by employing the trapezoidal rule as

$$u_k(x,t) = \frac{k}{2\pi \iota} \sum_{j=-M}^{M} e^{s_j t} \hat{u}(x,s_j) s_j', \quad \boldsymbol{\mu}_j = jk, s_j = s(\boldsymbol{\mu}_j), s_j' = s'(\boldsymbol{\mu}_j).\tag{18}$$

The solution $u_k(x,t)$, can be obtained by solving the system of equations in (11)–(12) in parallel for the nodes s_j. In order to do this we employ the meshless method in local setting for discretization of the operators $\mathcal{L}$ and $\mathcal{B}$.

3.1 Local meshless scheme

For data points $\{x_i\}_{i=1}^N$ in $\mathbb{R}^d$, $d \geq 1$ the local meshless approximation of $\hat{u}(x)$ is given by

$$\hat{u}(x_i) = \sum_{x_j \in \Omega_i} \lambda_j^i \phi\left(\left\|x_i - x_j^i\right\|\right), \tag{19}$$

where the vector $\boldsymbol{\lambda}^i = \{\lambda_j^i\}_{j=1}^n$ represents the expansion coefficients, $\phi(r)$ is kernel function and $r = \|x_i - x_j\|$ is the distance between x_i and x_j. Ω_i and Ω are local and global domains, respectively. The local domain Ω_i includes the center x_i and its n neighboring centers around it. Hence we have N $n \times n$ linear systems as

$$\begin{pmatrix} \hat{u}(x_1^i) \\ \hat{u}(x_2^i) \\ \vdots \\ \hat{u}(x_n^i) \end{pmatrix} = \begin{pmatrix} \phi(\|x_1^i - x_1^i\|) & \phi(\|x_1^i - x_2^i\|) & \cdots & \phi(\|x_1^i - x_n^i\|) \\ \phi(\|x_2^i - x_1^i\|) & \phi(\|x_2^i - x_2^i\|) & \cdots & \phi(\|x_2^i - x_n^i\|) \\ \vdots & \vdots & \vdots & \vdots \\ \phi(\|x_n^i - x_1^i\|) & \phi(\|x_n^i - x_2^i\|) & \cdots & \phi(\|x_n^i - x_n^i\|) \end{pmatrix} \begin{pmatrix} \lambda_1^i \\ \lambda_2^i \\ \vdots \\ \lambda_n^i \end{pmatrix},$$

$$i = 1, 2, \ldots, N, \tag{20}$$

which can be written as

$$\hat{\boldsymbol{u}}^i = \Phi^i \boldsymbol{\lambda}^i, \quad 1 \leq i \leq N, \tag{21}$$

where Φ^i is called the system matrix having entries of the form $b_{kj}^i = \phi(\|x_k^i - x_j^i\|)$, where $x_k^i, x_j^i \in \Omega_i$. Solving the N systems in Eq. (21) we obtain the unknowns $\boldsymbol{\lambda}^i = \{\lambda_j^i\}_{j=1}^n$. The differential operator $\mathcal{L}$ can be approximated as

$$\mathcal{L}\hat{u}(x_i) = \sum_{x_j \in \Omega_i} \lambda_j^i \mathcal{L}\phi\left(\left\|x_i - x_j^i\right\|\right), \tag{22}$$

Equation (22) can be written as

$$\mathcal{L}\hat{u}(x_i) = \boldsymbol{\lambda}^i \cdot \boldsymbol{\nu}^i, \tag{23}$$

where the vectors $\boldsymbol{\nu}^i$ and $\boldsymbol{\lambda}^i$ have orders $1 \times n$ and $n \times 1$, respectively. The entries of $\boldsymbol{\nu}^i$ are of the form

$$\boldsymbol{\nu}^i = \mathcal{L}\phi\left(\left\|x_i - x_j^i\right\|\right), \quad x_j^i \in \Omega_i, \tag{24}$$

solving Eq. (21) and Eq. (23) for $\boldsymbol{\lambda}^i$, we have

$$\mathcal{L}\hat{u}(x_i) = \boldsymbol{\nu}^i \left(\Phi^i\right)^{-1} \hat{\boldsymbol{u}}^i = \boldsymbol{\varpi}^i \hat{\boldsymbol{u}}^i, \tag{25}$$

where

$$\boldsymbol{\varpi}^i = \boldsymbol{\nu}^i \left(\Phi^i\right)^{-1}, \tag{26}$$

hence at each center x_i the operator $\mathcal{L}$ can be approximated via a local meshless method as

$$\mathcal{L}\hat{u} \equiv \mathbf{D}\hat{u}, \tag{27}$$

where $D_{N \times N}$ is a sparse system matrix obtained via meshless method in local setting approximating $\mathcal{L}$. We can approximate the operator $\mathcal{B}$ in a similar way.

4 Accuracy and convergence

The process of approximating the solution of the problem defined in Eq. (1)–Eq. (3) involves the transformation of the given equation by employing the Laplace transform, no error occurs in this process. Then we employ the meshless method in a local setting for solving the transformed problem. The error estimate is $O(\gamma^{\frac{1}{\epsilon h}})$, $0 < \gamma < 1$ (where h is the fill distance and ϵ is the shape parameter) for the meshless method in the local setting. Finally, we obtain the solution of the problem via the inverse Laplace transform by representing it as a Bromwich integral (17). The integral is then approximated to high accuracy via the trapezoidal rule. While approximating the integral (17) the convergence rate is dependent on Γ. Also in this process the convergence orders are dependent on the step k and on the chosen temporal domain $[t_0, T]$. For optimal results and best convergence we choose an optimal temporal domain. A proof of the error is given in the next theorem.

Theorem 1 ([40], Theorem 2.1) *Let* (6) *have solution $u(x,t)$ with $\hat{u}(x,s)$ analytic in Σ_ϕ^δ. Let $\Gamma \subset \Omega_r \subset \Sigma_\phi^\delta$, and define for $b > 0$, $\cosh(b) = (\eta\tau\sin(\theta))^{-1}$, where $0 < \tau_0 < T$, $\tau = \frac{t_0}{T}$, $0 < \eta < 1.0$ and let $\xi = \frac{\eta\bar{r}M}{bT}$. Then with $k = \frac{b}{M} \leq \frac{\bar{r}}{\log 2}$, for Eq. (18), we have $|u(x,t) - u_k(x,t)| \leq CQe^{\delta\tau}l(\|u_0\| + \|\widehat{\mathcal{H}}\|_{\Sigma_\phi^\delta})(\rho_r M)e^{-\mu M}$, for $\mu = \frac{\bar{r}(1-\eta)}{b}$, $\rho_r = \frac{\eta\bar{r}\tau\sin(\theta-r)}{b}$, $\bar{r} = 2\pi r$, $r > 0$, $\tau_0 \leq t \leq T$, $l(x) = \max(1, \log(\frac{1}{x}))$, and $C = C_{\delta,r,\phi}$. Hence we have*

$$error_{est} = \left|u_k(x,t) - u(x,t)\right| = O\left(e^{-\mu M}\right).$$

5 Stability of the method

For the stability of the system defined in Eq. (11)–Eq. (12), we write the system in matrix form given as

$$\boldsymbol{Q}\hat{u} = \mathfrak{R}, \tag{28}$$

where $\boldsymbol{Q}_{N \times N}$ is obtained via a local meshless method. The constant of stability for the system Eq. (28) is defined as

$$S_c = \sup_{\hat{u} \neq 0} \frac{\|\hat{u}\|}{\|\boldsymbol{Q}\hat{u}\|}, \tag{29}$$

for any discrete norm $\| \cdot \|$ defined on R^N the constant S_c is finite. From Eq. (29) we may write

$$\|\boldsymbol{Q}\|^{-1} \leq \frac{\|\hat{u}\|}{\|\boldsymbol{Q}\hat{u}\|} \leq S_c, \tag{30}$$

Figure 1 (**a**) The plot of the stability constant S_c for Example 2, with $N = 35$, $n = 9$, $M = 70$, and $\alpha = 0.3321$ at $t = 1$. We see that $1.3008 \leq S_c \leq 1.3504$. It is observed that the upper and lower bounds for the stability constant are very small numbers, which guarantees that the proposed localized meshless scheme is stable. (**b**) The contour of integration
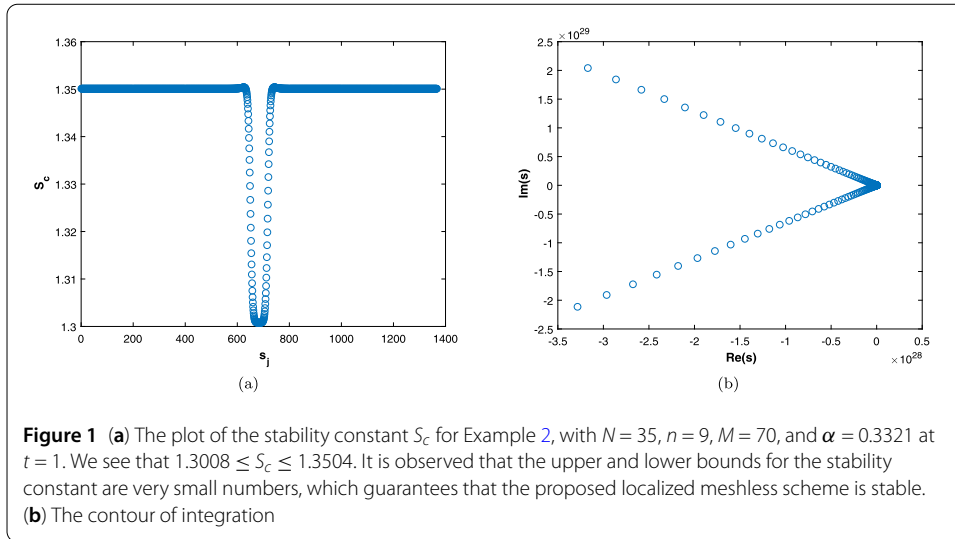
also for the pseudoinverse $\boldsymbol{Q}^{\dagger}$ of $\boldsymbol{Q}$, we have

$$\left\| \boldsymbol{Q}^{\dagger} \right\| = \sup_{\boldsymbol{B} \neq 0} \frac{\left\| \boldsymbol{Q}^{\dagger} \boldsymbol{B} \right\|}{\left\| \boldsymbol{B} \right\|}. \tag{31}$$

Thus, we have

$$\left\| \boldsymbol{Q}^{\dagger} \right\| \geq \sup_{\boldsymbol{B} = \boldsymbol{Q}\hat{\boldsymbol{B}} \neq 0} \frac{\left\| \boldsymbol{Q}^{\dagger} \boldsymbol{Q} \hat{\boldsymbol{u}} \right\|}{\left\| \boldsymbol{Q} \hat{\boldsymbol{u}} \right\|} = \sup_{\hat{\boldsymbol{u}} \neq 0} \frac{\left\| \hat{\boldsymbol{u}} \right\|}{\left\| \boldsymbol{Q} \hat{\boldsymbol{u}} \right\|} = S_c. \tag{32}$$

From Eq. (30) and Eq. (32) we observe that the constant S_c is bounded. Calculation of the pseudoinverse for the system (28) may be computationally expensive, but it confirms the stability. For square matrices we can use the MATLAB's function condest for estimating $\| \boldsymbol{Q}^{-1} \|_{\infty}$, hence we have

$$S_c = \frac{\text{condest}(\boldsymbol{Q}')}{\| \boldsymbol{Q} \|_{\infty}} \tag{33}$$

For our sparse matrix $\boldsymbol{Q}$ this works well in a very short time of computation (Fig.1).

6 Numerical experiments

Here we employ our proposed numerical scheme for the approximations different one dimensional linear PDEs. For optimization of the shape parameter we have utilized the uncertainty principle due to [41]. In our numerical experiments for generating the quadrature nodes the command $\boldsymbol{\mu} = -M : k : M$ is used, also the multiquadrics (MQ) kernel is used in all experiments. Other optimal parameters involved for the contour of integration are $\theta = 0.15410$, $r = 0.13870$, $\eta = 0.10$, $\tau = \frac{t0}{T}$, $\delta = 2.0$, $t \in [t_0, T] = [0.5, 5]$. The accuracy of the method is measured via the L_{∞} error given by

$$L_{\infty} = \left\| u(x, t) - u_k(x, t) \right\|_{\infty} = \max_{1 \leq j \leq N} \left(\left| u(x, t) - u_k(x, t) \right| \right).$$

Here $u(x, t)_k$ and $u(x, t)$ are the numerical and exact solutions respectively.

Table 1 The results are obtained for $\alpha = 0.22111$, $x \in [0, 1]$, and $t = 1$

N	n	M	L_∞	$error_{est}$	ε	κ	C.time(s)
40	5	30	7.55×10^{-2}	5.37×10^{-1}	1.9	$1.14 \times 10^{+10}$	0.229707
		40	1.10×10^{-3}	1.83×10^{-1}	1.9	$1.14 \times 10^{+10}$	0.327267
		50	4.30×10^{-3}	6.25×10^{-2}	1.9	$1.14 \times 10^{+10}$	0.488246
		60	3.63×10^{-4}	2.12×10^{-2}	1.9	$1.14 \times 10^{+10}$	0.711818
		70	2.15×10^{-4}	7.20×10^{-3}	1.9	$1.14 \times 10^{+10}$	1.416137
		80	4.94×10^{-5}	2.40×10^{-4}	1.9	$1.14 \times 10^{+10}$	3.252525
		90	1.36×10^{-5}	8.18×10^{-4}	1.9	$1.14 \times 10^{+10}$	5.078051
60	5	90	4.84×10^{-5}	8.18×10^{-4}	2.9	$1.06 \times 10^{+10}$	9.992066
	10		8.73×10^{-5}	8.18×10^{-4}	7.4	$1.18 \times 10^{+10}$	7.996995
	15		5.99×10^{-4}	8.18×10^{-4}	8.9	$1.02 \times 10^{+10}$	10.601678
10	8	90	7.81×10^{-5}	8.18×10^{-4}	0.9	$2.26 \times 10^{+10}$	0.577473
20			2.97×10^{-5}	8.18×10^{-4}	2.0	$1.18 \times 10^{+10}$	1.026700
30			5.30×10^{-5}	8.18×10^{-4}	3.0	$1.47 \times 10^{+10}$	2.842371
35			8.95×10^{-5}	8.18×10^{-4}	3.6	$1.10 \times 10^{+10}$	4.340015

(a)   (b)

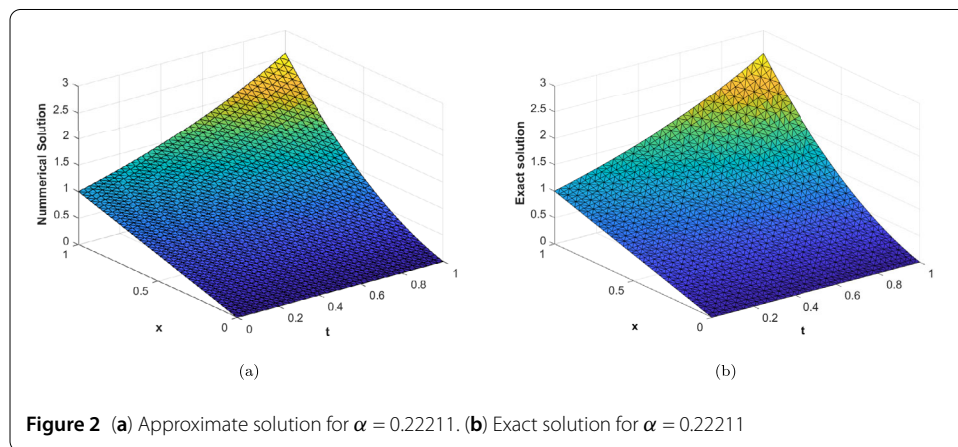**Figure 2** (**a**) Approximate solution for $\alpha = 0.22211$. (**b**) Exact solution for $\alpha = 0.22211$

Example 1 Here we consider a 1-D linear differential equation with the CF derivative [2]

$$\,_0^{CF}D_t^{\alpha+1}u(x,t) - \frac{1}{2}x^2 D_{xx}u(x,t) = 0, \quad x,t,\alpha \in (0,1) \text{ where } D_{xx} = \frac{\partial^2}{\partial x^2}. \tag{34}$$

the initial conditions are

$$u(x,0) = x, \qquad D_t u(x,0) = x^2. \tag{35}$$

The boundary conditions are extracted from the exact solution

$$u(x,t) = x + x^2 \left(\frac{e^t - e^{-\alpha t}}{1 + \alpha} \right). \tag{36}$$

The results obtained for different centers n in local domain Ω_i and N in global domain Ω are given in Table 1 for fractional order $\alpha = 0.22211$ and various quadrature points. The condition number κ, L_∞ errors, shape parameter ε, and the error estimates are also given in Table 1. From Table 1 it is clear that the proposed method gives an acceptable accuracy. The approximate and exact solutions are plotted in Fig. 2(a) and Fig. 2(b), respectively, which clearly shows good agreement between them. The contour plot of absolute error is shown in Fig. 3(a), which shows a high accuracy. The plot of actual error vs error estimate
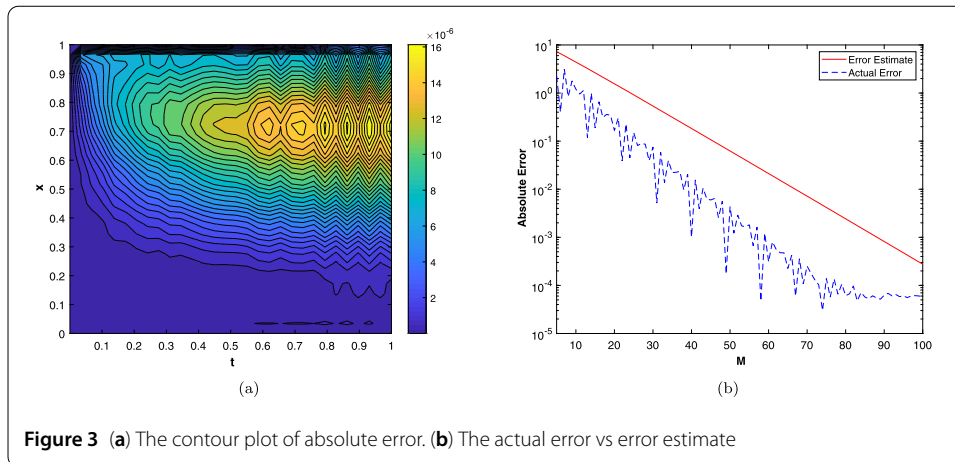
Figure 3 (**a**) The contour plot of absolute error. (**b**) The actual error vs error estimate

Table 2 The results are obtained for $\alpha = 0.3321$, $x \in [0, 1]$, and $t = 1$

N	n	M	L_∞	$error_{est}$	ε	κ	C.time(s)
45	5	30	1.10×10^{-1}	5.37×10^{-1}	2.1	$1.34 \times 10^{+10}$	0.133238
		50	5.30×10^{-3}	6.25×10^{-2}	2.1	$1.34 \times 10^{+10}$	0.296257
		70	2.27×10^{-4}	7.20×10^{-3}	2.1	$1.34 \times 10^{+10}$	0.620503
		90	8.22×10^{-5}	8.18×10^{-4}	2.1	$1.34 \times 10^{+10}$	3.566523
40	5	90	4.78×10^{-4}	8.18×10^{-4}	1.08	$1.01 \times 10^{+12}$	2.989985
	8		8.31×10^{-5}	8.18×10^{-4}	2.9	$1.04 \times 10^{+12}$	3.039480
	10		7.93×10^{-5}	8.18×10^{-4}	3.65	$1.0 \times 10^{+12}$	2.642598
35	9	90	1.10×10^{-4}	8.18×10^{-4}	2.88	$1.03 \times 10^{+12}$	2.187149
40		90	5.54×10^{-5}	8.18×10^{-4}	3.31	$1.0 \times 10^{+12}$	2.800518
50		90	9.07×10^{-5}	8.18×10^{-4}	4.16	$1.0 \times 10^{+12}$	4.435288

is shown in Fig. 3(b), which shows good agreement between them. From the results we conclude that the proposed method is effective.

Example 2 Here we consider a non-homogeneous linear differential equation with the CF derivative [2]:

$$\,^{CF}_{0}D_t^\alpha u(x,t) + xD_x u(x,t) + D_{xx} u(x,t) = 2\big(t^2 + x^2 + 1\big), \quad x, t, \alpha \in (0,1). \tag{37}$$
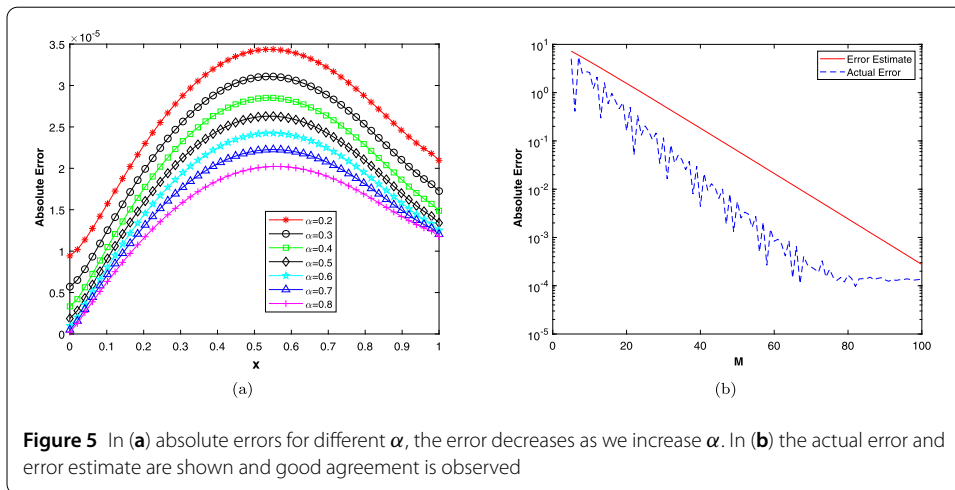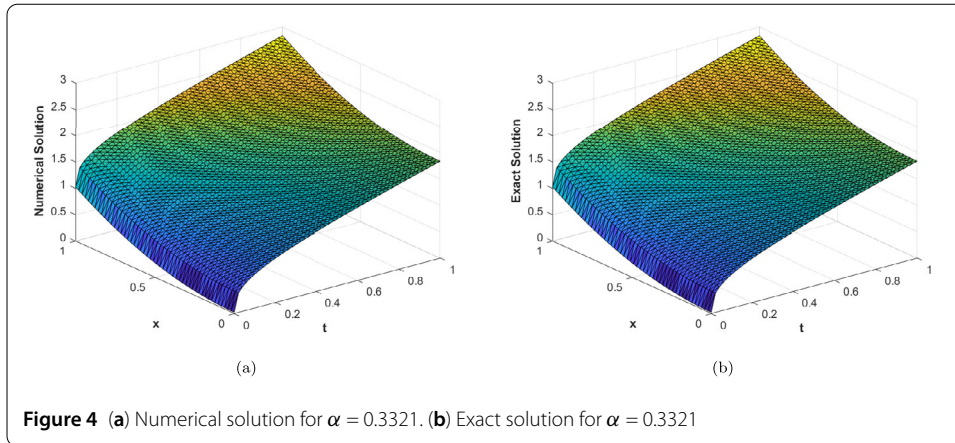
the initial condition being

$$u(x,0) = x^2, \tag{38}$$

the boundary conditions can be obtained from the exact solution

$$u(x,t) = x^2 + \frac{2t^\alpha(1 + (t - \alpha)\alpha)}{1 + \alpha}. \tag{39}$$

The results obtained for different centers n in local domain Ω_i and N in global domain Ω are shown in Table 2 with fractional order $\alpha = 0.22211$ and various quadrature nodes. From the observations on this table also we conclude that the results obtained using the proposed numerical scheme are acceptable. The plots of exact and approximate solutions are given in Fig. 4(a), and Fig. 4(b), respectively. The error functions for different values of α are shown in Fig. 5(a), we observe that the error decreases as we increase α. In Fig. 5(b)

Figure 4 (**a**) Numerical solution for $\alpha = 0.3321$. (**b**) Exact solution for $\alpha = 0.3321$

Figure 5 In (**a**) absolute errors for different α, the error decreases as we increase α. In (**b**) the actual error and error estimate are shown and good agreement is observed

the actual error and error estimates are shown, which shows good agreement between them.

Example 3 Next the 1-D non-homogeneous diffusion equation with the CF derivative is considered:

$$\,_0^{CF}D_t^\alpha u(x,t) + D_{xx}u(x,t) = h(x,t), \quad -1 < x < 1, 0 < t < 10 < \alpha \le 1. \tag{40}$$

with the forcing term

$$h(x,t) = \frac{1}{1-\alpha}\sin(2\pi x)\left(\frac{3t^2}{\boldsymbol{P}} - \frac{6t}{\boldsymbol{P}^2} + \frac{6}{\boldsymbol{P}^3}\left(1 - e^{-\boldsymbol{P}t}\right)\right)$$
$$+ 4\pi^2\left(t^3 + 1\right)\sin(2\pi x), \quad \text{where } \boldsymbol{P} = \frac{\alpha}{1-\alpha}. \tag{41}$$

The problem has the following exact solution:

$$u(x,t) = \sin(2\pi x)\left(t^3 + 1\right). \tag{42}$$

Table 3 The results are obtained for $\alpha = 0.3$, $x \in [-1, 1]$, and $t = 1$

N	n	M	L_∞	$error_{est}$	ε	κ	C.time(s)
60	10	30	0.1103	0.5373	2.7	$1.42 \times 10^{+12}$	0.118417
		50	6.30×10^{-3}	6.25×10^{-2}	2.7	$1.42 \times 10^{+12}$	0.325090
		70	3.42×10^{-4}	7.20×10^{-3}	2.7	$1.42 \times 10^{+12}$	1.494413
		90	8.67×10^{-5}	8.18×10^{-4}	2.7	$1.42 \times 10^{+12}$	5.319907
		100	8.53×10^{-5}	2.76×10^{-4}	2.7	$1.42 \times 10^{+12}$	8.300325
10	10	90	0.1088	8.18×10^{-4}	0.4	$2.26 \times 10^{+12}$	0.318351
30			4.84×10^{-4}	8.18×10^{-4}	1.3	$1.97 \times 10^{+12}$	0.993061
50			1.64×10^{-4}	8.18×10^{-4}	2.2	$1.93 \times 10^{+12}$	4.045085
60			8.67×10^{-5}	8.18×10^{-4}	2.7	$1.42 \times 10^{+12}$	5.298335
80	10	100	1.92×10^{-4}	2.76×10^{-4}	3.6	$1.52 \times 10^{+12}$	11.975305
	15		1.24×10^{-4}	2.76×10^{-4}	4.6	$1.14 \times 10^{+12}$	12.048443
	20		4.90×10^{-5}	2.76×10^{-4}	5.0	$1.13 \times 10^{+12}$	12.145290

Table 4 The results are obtained for $\alpha = 0.7$, $x \in [-1, 1]$, and $t = 1$

N	n	M	L_∞	$error_{est}$	ε	κ	C.time(s)
60	10	30	0.1103	5.37×10^{-1}	2.7	$1.42 \times 10^{+12}$	0.137554
		40	2.10×10^{-3}	1.83×10^{-1}	2.7	$1.42 \times 10^{+12}$	0.194359
		60	5.01×10^{-4}	2.12×10^{-2}	2.7	$1.42 \times 10^{+12}$	0.557261
		70	1.03×10^{-4}	2.40×10^{-3}	2.7	$1.42 \times 10^{+12}$	3.174273
		90	8.49×10^{-5}	8.18×10^{-4}	2.7	$1.42 \times 10^{+12}$	5.439579
20	15	90	3.0×10^{-3}	8.18×10^{-4}	1.1	$1.28 \times 10^{+12}$	0.522960
40			3.37×10^{-4}	8.18×10^{-4}	2.2	$2.14 \times 10^{+12}$	2.770111
60			1.75×10^{-4}	8.18×10^{-4}	1.4	$3.40 \times 10^{+12}$	5.318668
70			8.76×10^{-5}	8.18×10^{-4}	4	$1.24 \times 10^{+12}$	6.681699
60	5	90	1.95×10^{-4}	8.18×10^{-4}	0.8	$1.20 \times 10^{+12}$	5.343147
	8		9.18×10^{-5}	8.18×10^{-4}	2.2	$1.00 \times 10^{+12}$	5.416387
	10		8.49×10^{-5}	8.18×10^{-4}	2.7	$1.42 \times 10^{+12}$	5.488575
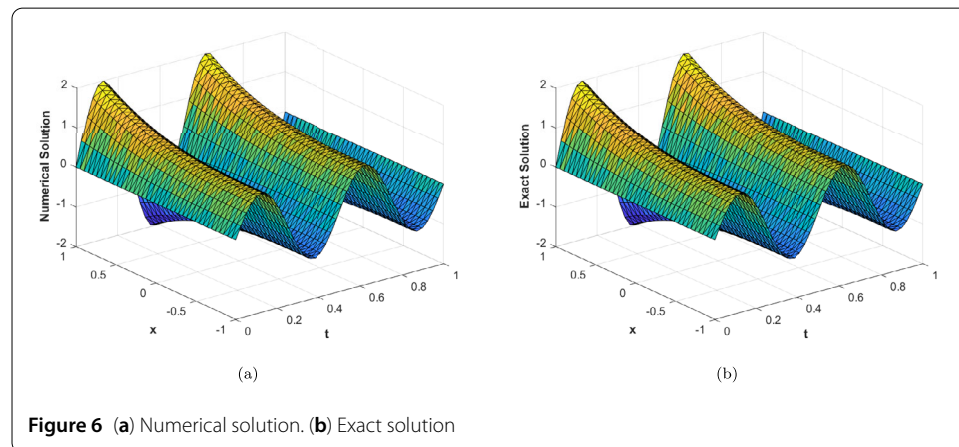
Figure 6 (**a**) Numerical solution. (**b**) Exact solution

The initial and boundary conditions are extracted from the exact solution. The results obtained for different nodes $n \in \Omega_i$, $N \in \Omega$ and different quadrature nodes with $\alpha = 0.3$, $\alpha = 0.7$ are shown Table 3 and Table 4. A clear improvement is observed in the accuracy as we increase the spatial and quadrature nodes. The plots of exact and numerical solutions are given in Fig. 6(a) and in Fig. 6(b). In Fig. 7(a) the contour plot of the absolute error is given, which shows a high accuracy of the proposed numerical scheme. In Fig. 7(b) the plot of the actual error and error estimate is shown, which shows good agreement between them. The results ensure the convergence, stability, and efficiency of our method.
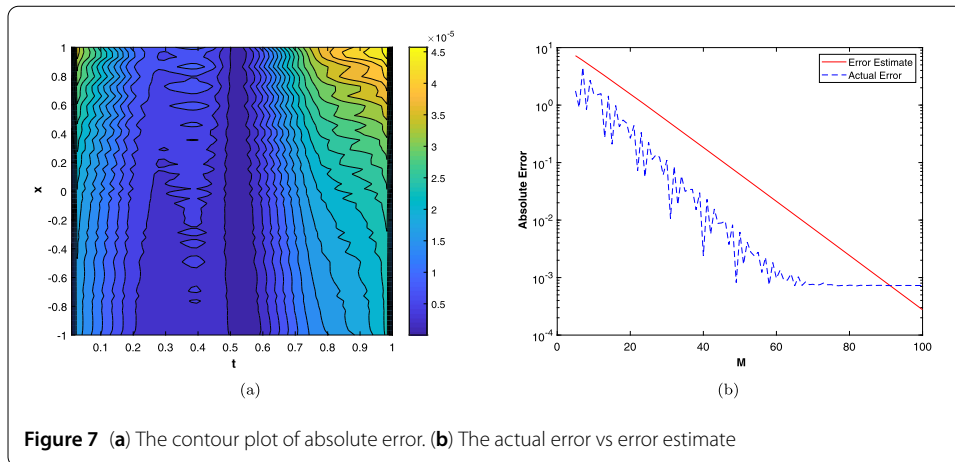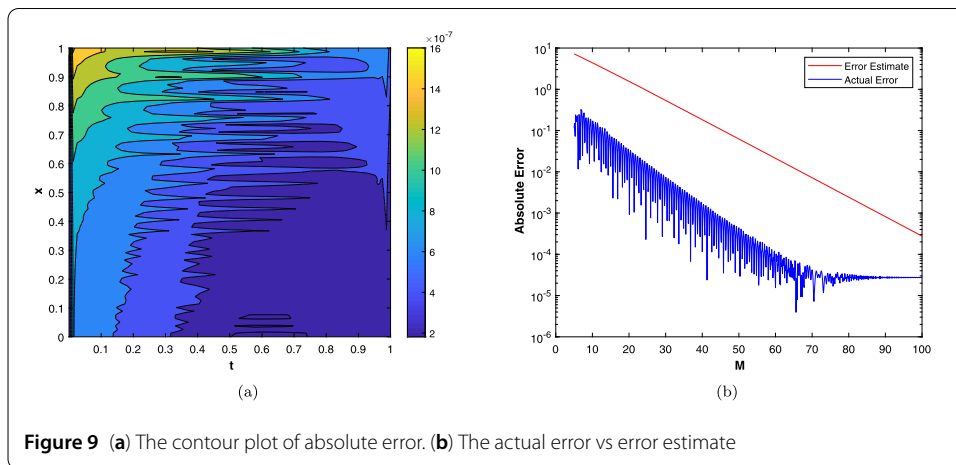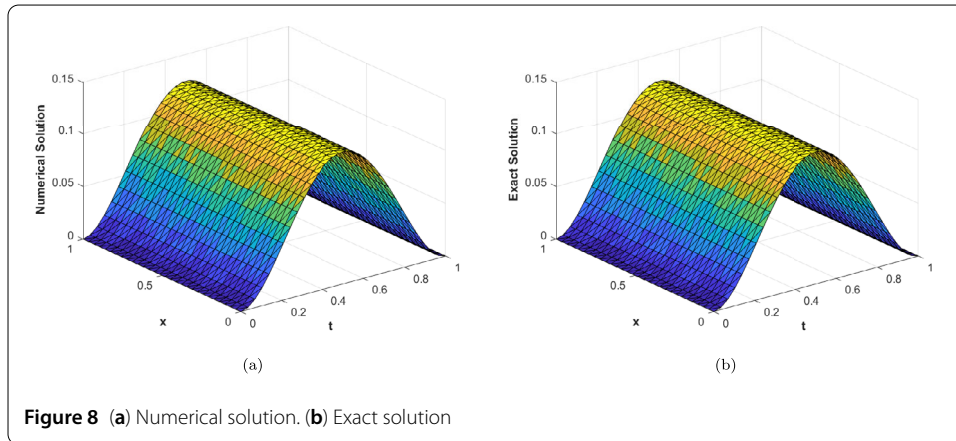
Figure 7 (**a**) The contour plot of absolute error. (**b**) The actual error vs error estimate

Example 4 The next test problem is the 1-D non-homogeneous diffusion equation with the CF derivative:

$$
{}_0^{CF}D_t^\alpha u(x,t) + D_{xx}u(x,t) = h(x,t), \quad \chi, \tau, \alpha \in (0,1). \tag{43}
$$

The initial condition is

$$
u(x,0) = x^2\left(1 - x^2\right), \tag{44}
$$

with the forcing term

$$
\begin{aligned}
h(x,t) &= \frac{1}{1-\alpha}x^2(1-x)^2\left(\frac{3t^2}{P} - \frac{6t}{P^2} + \frac{6}{P^3}\left(1 - e^{-Pt}\right)\right) \\
&\quad - \left(t^3 + 1\right)\left(12x^2 - 12x + 2\right), \quad \text{where } P = \frac{\alpha}{1-\alpha}.
\end{aligned} \tag{45}
$$

The exact solution is

$$
u(x,t) = \left(t^3 + 1\right)x^2(1-x)^2. \tag{46}
$$

The initial and boundary conditions are extracted from the exact solution. The results obtained for different nodes $n \in \Omega_i$, $N \in \Omega$ and different quadrature nodes with $\alpha = 0.7$ are given Table 5. The plots of exact and numerical solutions are given in Fig. 8(a) and in Fig. 8(b). In Fig. 9(a) the contour plot of absolute error is shown, and in Fig. 9(b) the plot of actual error vs error estimate is shown, which shows good agreement between them. For this problem also the method produced accurate and stable results.

7 Conclusion

In this work, we have coupled the Laplace transform and a meshless method in a local setting successfully for the approximation of linear one dimensional partial differential equations with the CF derivative. The Laplace transform reduced the problem to a time independent problem and in this way the classical time stepping procedure and hence the

Table 5 The results are obtained for $\alpha = 0.7$, $x \in [0, 1]$, and $t = 1$

N	n	M	L_∞	$error_{est}$	ε	κ	C.time(s)
70	15	30	6.70×10^{-3}	5.37×10^{-1}	8.0	$1.24 \times 10^{+12}$	0.264581
		50	3.82×10^{-4}	6.25×10^{-2}	8.0	$1.24 \times 10^{+12}$	0.603418
		70	1.90×10^{-5}	7.20×10^{-3}	8.0	$1.24 \times 10^{+12}$	1.098719
		90	5.38×10^{-6}	8.18×10^{-4}	8.0	$1.24 \times 10^{+12}$	2.220157
30	10	80	2.06×10^{-5}	2.40×10^{-3}	2.7	$1.08 \times 10^{+12}$	0.800305
50			1.23×10^{-5}	2.40×10^{-3}	4.5	$1.35 \times 10^{+12}$	1.135721
70			2.22×10^{-5}	2.40×10^{-3}	6.4	$1.15 \times 10^{+12}$	1.567001
80			5.16×10^{-6}	2.40×10^{-3}	7.3	$1.22 \times 10^{+12}$	1.787725

Figure 8 (**a**) Numerical solution. (**b**) Exact solution

Figure 9 (**a**) The contour plot of absolute error. (**b**) The actual error vs error estimate

time instability issues were avoided. The local meshless method produced sparse differentiation matrices and the issues of ill conditioning and shape parameter sensitivity were resolved. We discussed the convergence and stability of the method. Some numerical experiments were performed on one dimensional problems with a CF derivative for different fractional orders. Numerical results confirmed the stability and high accuracy of the proposed method. The obtained results ensured the efficiency and applicability of the method for such problems.

Author details
^{1}Department of Mathematics, Islamia College Peshawar, Khyber Pakhtoon Khwa, Pakistan. ^{2}Institute of IR 4.0, The National University of Malaysia, 43600 UKM, Bangi, Selangor, Malaysia. ^{3}Positive Computing Research Group, Institute of Autonomous Systems, Department of Computer & Information Sciences, Universiti Teknologi Petronas, 32610, Bandar Seri Iskandar, Perak, Malaysia. ^{4}Young Researchers and Elite Club, Mobarakeh Branch, Islamic Azad University, Mobarakeh, Iran. ^{5}Faculty of Engineering and Natural Sciences, Bahcesehir University, Istanbul, Turkey.

Publisher's Note
Springer Nature remains neutral with regard to jurisdictional claims in published maps and institutional affiliations.

References
1. Atangana, A., Alkahtani, B.S.T.: New model of groundwater flowing within a confine aquifer: application of Caputo–Fabrizio derivative. Arab. J. Geosci. **9**(1), 8 (2016)
2. Morales-Delgado, V.F., Gómez-Aguilar, J.F., Yépez-Martínez, H., Baleanu, D., Escobar-Jimenez, R.F., Olivares-Peregrino, V.H.: Laplace homotopy analysis method for solving linear partial differential equations using a fractional derivative with and without kernel singular. Adv. Differ. Equ. **2016**(1), 164 (2016)
3. Shah, K., Seadawy, A.R., Arfan, M.: Evaluation of one dimensional fuzzy fractional partial differential equations. Alex. Eng. J. **59**(5), 3347–3353 (2020)
4. Khan, H., Shah, R., Kumam, P., Arif, M.: Analytical solutions of fractional-order heat and wave equations by the natural transform decomposition method. Entropy **21**(6), 597 (2019)
5. Liu Kamran, X., Yao, Y.: Numerical approximation of Riccati fractional differential equation in the sense of Caputo-type fractional derivative. J. Math. **2020**, Article ID 1274251 (2020)
6. Adigüzel, R.S., Aksoy, Ü., Karapinar, E., Erhan, İ.M.: On the solution of a boundary value problem associated with a fractional differential equation. Math. Methods Appl. Sci. (2020). https://doi.org/10.1002/mma.6652
7. Afshari, H., Kalantari, S., Karapinar, E.: Solution of fractional differential equations via coupled fixed point. Electron. J. Differ. Equ. **286**, 2015 (2015)
8. Samko, S.G., Kilbas, A.A., Marichev, O.I.: Fractional Integrals and Derivatives, vol. 1993. Gordon & Breach, Yverdon Yverdon-les-Bains (1993)
9. Podlubny, I.: Fractional Differential Equations: An Introduction to Fractional Derivatives, Fractional Differential Equations, to Methods of Their Solution and Some of Their Applications, vol. 198. Elsevier, Amsterdam (1998)
10. Kilbas, A.A., Srivastava, H.M., Trujillo, J.J.: Theory and Applications of Fractional Differential Equations, vol. 204. Elsevier, Amsterdam (2006)
11. Patil, J., Chaudhari, A., Mohammed, A., Hardan, B.: Upper and lower solution method for positive solution of generalized Caputo fractional differential equations. Adv. Theory Nonlinear Anal. Appl. **4**(4), 279–291 (2020)
12. Muthaiah, S., Murugesan, M., Thangaraj, N.G.: Existence of solutions for nonlocal boundary value problem of Hadamard fractional differential equations. Adv. Theory Nonlinear Anal. Appl. **3**(3), 162–173 (2019)
13. Karapinar, E., Binh, H.D., Luc, N.H., Can, N.H.: On continuity of the fractional derivative of the time-fractional semilinear pseudo-parabolic systems. Adv. Differ. Equ. **2021**(1), 1 (2021)
14. Afshari, H., Karapınar, E.: A discussion on the existence of positive solutions of the boundary value problems via ψ-Hilfer fractional derivative on b-metric spaces. Adv. Differ. Equ. **2020**(1), 1 (2020)
15. Salim, A., Benchohra, M., Lazreg, J.E., Henderson, J.: Nonlinear implicit generalized Hilfer-type fractional differential equations with non-instantaneous impulses in Banach spaces. Adv. Theory Nonlinear Anal. Appl. **4**(4), 332–348 (2020)
16. Khan, H., Khan, A., Jarad, F., Shah, A.: Existence and data dependence theorems for solutions of an ABC-fractional order impulsive system. Chaos Solitons Fractals **131**, 109477 (2020)
17. Caputo, M., Fabrizio, M.: A new definition of fractional derivative without singular kernel. Prog. Fract. Differ. Appl. **1**(2), 1–13 (2015)
18. Cruz-Duarte, J.M., Rosales-Garcia, J., Correa-Cely, C.R., Garcia-Perez, A., Avina-Cervantes, J.G.: A closed form expression for the Gaussian-based Caputo–Fabrizio fractional derivative for signal processing applications. Commun. Nonlinear Sci. Numer. Simul. **61**, 138–148 (2018)
19. Atangana, A., Alqahtani, R.T.: Numerical approximation of the space-time Caputo–Fabrizio fractional derivative and application to groundwater pollution equation. Adv. Differ. Equ. **2016**(1), 156 (2016)
20. Feulefack, P.A., Djida, J.D., Atangana, A.: A new model of groundwater flow within an unconfined aquifer: application of Caputo–Fabrizio fractional derivative. Discrete Contin. Dyn. Syst., Ser. B **24**(7), 3227–3247 (2019)
21. Gómez-Aguilar, J.F., Yépez-Martínez, H., Calderón-Ramón, C., Cruz-Orduña, I., Escobar-Jiménez, R., Olivares-Peregrino, V.: Modeling of a mass-spring-damper system by fractional derivatives with and without a singular kernel. Entropy **17**(9), 6289–6303 (2015)

22. Zhou, H.W., Yang, S., Zhang, S.Q.: Modeling non-Darcian flow and solute transport in porous media with the Caputo–Fabrizio derivative. Appl. Math. Model. **68**, 603–615 (2019)
23. Korpinar, Z.: On numerical solutions for the Caputo–Fabrizio fractional heat-like equation. Therm. Sci. **22**(Suppl. 1), 87–95 (2018)
24. Atangana, A.: On the new fractional derivative and application to nonlinear Fisher's reaction–diffusion equation. Appl. Math. Comput. **273**, 948–956 (2016)
25. Algahtani, O.J.J.: Comparing the Atangana–Baleanu and Caputo–Fabrizio derivative with fractional order: Allen Cahn model. Chaos Solitons Fractals **89**, 552–559 (2016)
26. Mirza, I.A., Vieru, D.: Fundamental solutions to advection–diffusion equation with time-fractional Caputo–Fabrizio derivative. Comput. Math. Appl. **73**(1), 1–10 (2017)
27. Goufo, E.F.D., Pene, M.K., Mwambakana, J.N.: Duplication in a model of rock fracture with fractional derivative without singular kernel. Open Math. **13**(1), 839–846 (2015)
28. Owolabi, K.M., Atangana, A.: Numerical approximation of nonlinear fractional parabolic differential equations with Caputo–Fabrizio derivative in Riemann–Liouville sense. Chaos Solitons Fractals **99**, 171–179 (2017)
29. Owolabi, K.M., Atangana, A.: Analysis and application of new fractional Adams–Bashforth scheme with Caputo–Fabrizio derivative. Chaos Solitons Fractals **105**, 111–119 (2017)
30. Goufo, E.F.D.: Application of the Caputo–Fabrizio fractional derivative without singular kernel to Korteweg–de Vries–Burgers equation. Math. Model. Anal. **21**(2), 188–198 (2016)
31. Cattani, C., Srivastava, H.M., Yang, X.J.: Fractional Dynamics. Sciendo Migration (2015)
32. Uddin Kamran, M., Ali, A.: A localized transform-based meshless method for solving time fractional wave-diffusion equation. In: Engineering Analysis with Boundary Elements (2017)
33. Kamran, Ali, G., Gómez-Aguilar, J.F.: Approximation of partial integro differential equations with a weakly singular kernel using local meshless method. Alex. Eng. J. **59**(4), 2091–2100 (2020)
34. Oldham, K.B., Spanier, J.: The Fractional Calculus Theory and Applications of Differentiation and Integration to Arbitrary Order, vol. 111. Academic Press, New York (1974)
35. Ngoc Thach, T., Can, N.H., Viet Tri, V.: Identifying the initial state for a parabolic diffusion from their time averages with fractional derivative. Math. Methods Appl. Sci. (2020). https://doi.org/10.1002/mma.7179
36. Can, N.H., Luc, N.H., Baleanu, D., Zhou, Y.: Inverse source problem for time fractional diffusion equation with Mittag-Leffler kernel. Adv. Differ. Equ. **2020**(1), 1 (2020)
37. Luc, N.H., Baleanu, D., Can, N.H.: Reconstructing the right-hand side of a fractional subdiffusion equation from the final data. J. Inequal. Appl. **2020**(1), 1 (2020)
38. Baitiche, Z., Derbazi, C., Benchohra, M.: ψ-Caputo fractional differential equations with multi-point boundary conditions by topological degree theory. Results Nonlinear Anal. **3**(4), 166–178 (2020)
39. Jarad, F., Abdeljawad, T.: A modified Laplace transform for certain generalized fractional operators. Results Nonlinear Anal. **1**(2), 88–98 (2018)
40. McLean, W., Thomee, V.: Numerical solution via Laplace transforms of a fractional order evolution equation. J. Integral Equ. Appl. **22**(1), 57–94 (2010)
41. Schaback, R.: Error estimates and condition numbers for radial basis function interpolation. Adv. Comput. Math. **3**, 251–264 (1995)